REMOTE SENSING OF ATMOSPHERE, HYDROSPHERE, AND UNDERLYING SURFACE

Experimental Study of the Reflection of Light Radiation from Crystalline Particles in the Lower Troposphere

**V. P. Galileiskii[a], A. I. Grishin[a], A. I. Elizarov[a], A. V. Kruchkov[a], *,
G. G. Matvienko[a], †, and A. M. Morozov[a]**

[a] *V.E. Zuev Institute of Atmospheric Optics, Siberian Branch, Russian Academy of Sciences, Tomsk, 634055 Russia*
*e-mail: kaw@iao.ru

Abstract—We considered the phenomenon of reflection of light radiation from crystalline particles preferentially oriented in the atmosphere, as well as the physical patterns and possible conditions favoring this reflection. Experimental observations were used to analyze the recorded light spots, occurring due to reflection of radiation from layers of these particles. We describe a case of recording specular layers using a panoramic optical station (AllSky system).

INTRODUCTION

The Earth's atmosphere contains a large amount of water in three phase states: vapor, liquid, and ice. The water phase state in each specific volume of the atmosphere is determined by the temperature, humidity, and atmospheric pressure. These parameters depend on the altitude, latitude of the site, season, as well as on the time in regard to convective and global air mass transports. As a consequence of these atmospheric processes, water experiences continuous mutual transitions from one phase state to another.

The morphologic features of water phase states affect appreciably the character of the optical radiation propagation in the atmosphere. At temperatures of 0°C and below, water transits from vapor and liquid phases into the solid state, i.e., ice. In contrast to liquid water (fog, raindrops), forming ice particles may greatly vary in shape: from large frozen agglomerate cores or snowflakes to almost geometrically ideal ice crystals shaped as prisms and hexagonal plates [1]. The temperature and water vapor content of the medium strongly influence the ice particle formation. Plates prevail if water freezes at weakly negative temperatures (0 to −4°C) in a wide range of water vapor pressure. Preferential orientation of ice crystal particles, with their flat facets aligned in the horizontal direction, can favor the occurrence of atmospheric specular reflection and other phenomena. Platt [2] was first to observe the light reflection from horizontally oriented crystals in atmospheric sensing.

The character of motion of crystalline particles in the Earth's atmosphere is determined by the two most significant factors: the gravitational effect of the planet and atmospheric airflow circumventing the particles [3]. In a calm atmosphere, each particle is in free fall as a result of the action of the force of gravity and air resistance. This fall may either be stable or unstable in character. When falling steadily (unsteadily), nonspherical particles are preferably (chaotically) oriented. Atmospheric airflow circumventing particles can either be laminar or turbulent. However, turbulence is always significantly reduced in the region of temperature inversions. In this case, nonspherical particles begin to orient themselves so as their largest aerodynamic size is perpendicular to the direction of motion. The spatial orientation of crystalline particles unavoidably leads to anisotropy of the physical properties of the atmosphere in which these crystals reside.

In practice, the specular reflection can readily and reliably be recorded by an observer if he is in the same plane as the optical radiation, incident on and reflected from the layer, taking into account the law of equality of the angles of incidence and reflection [4]. The temporal stability of specular reflection depends on the stability of the spatial orientation of the ensemble of ice crystals. In this case, a virtual image of the light source should be observed against the background of diffuse scattering from molecules and aerosol. The variations in reflective properties of this layer are explained by the variety of forms of ice crystals, variations in their concentrations and orientations in the irradiated volume, and the presence of particles
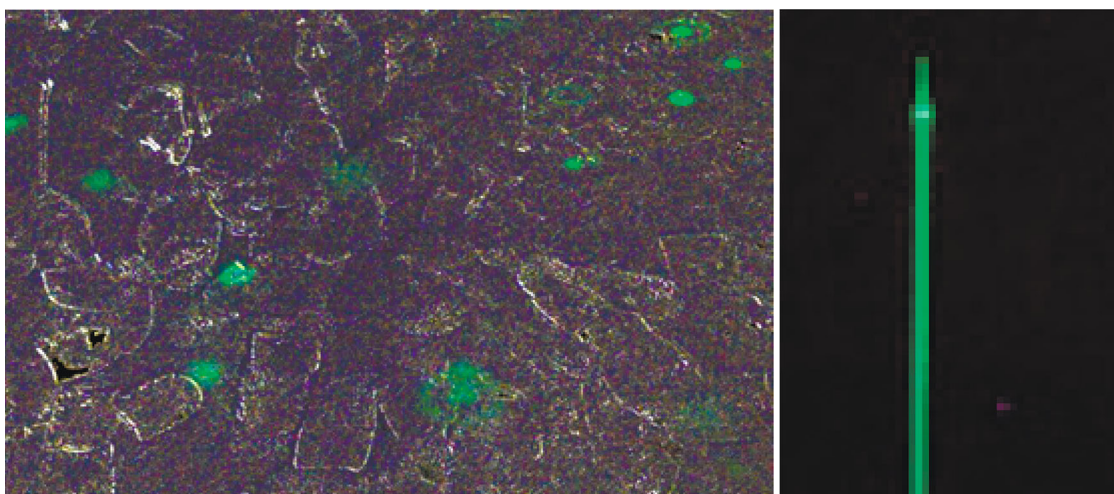
---

† Deceased.

Fig. 1. Image of light beams due to reflection of laser radiation from the specular layer of crystalline particles (left panel). Image of propagation of laser radiation in the aerosol atmosphere; in the upper part, we can discern enhanced-scattering layer (right panel).

devoid of the specular properties. Despite the fact that the specular reflection from ice crystals has quite a trivial nature, this phenomenon is rarely observed under natural atmospheric conditions.

In this paper, we present the results of lidar sensing and of the study of the atmosphere with a panoramic optical station (AllSky system). The combination of active (lidar sensing) and passive (AllSky camera) methods allows us to study specular reflection from ice crystals in different aspects. The AllSky camera makes it possible to merely fix the presence of reflecting layer and track its time dynamics (at least at the "yes/no" level); in contrast, active sensing makes it possible to determine the altitude, thickness, and configuration (sizes) of the specular reflection layer.

REFLECTION OF LASER RADIATION FROM ICE CRYSTALS IN THE ATMOSPHERE

Among the well-known methods for remote sensing of near-Earth outer (including air) space, the most promising are those based on the interaction between

Table 1. Characteristics of the atmospheric surface layer during sensing

Characteristic	Value
Surface air temperature	−18°C
Relative air humidity	65%
Wind direction	230° (W–SW)
Wind speed	1–3 m/s
Altitude of enhanced-scattering layer above ground	160 m
Thickness of enhanced-scattering layer	15 m

laser radiation and matter. The methods and means for monitoring and control of atmospheric space have been developed for many years in V.E. Zuev Institute of Atmospheric Optics, Siberian Branch, Russian Academy of Sciences (IAO SB RAS). They make it possible to rapidly acquire the most comprehensive information on entities in space under study, ensure high spatial resolution, and can provide information on the spectral distribution of particle sizes.

When optical radiation propagates in an atmosphere containing ice crystals, many optical phenomena are observed which primarily depend on the parameters of the atmospheric layer through which the optical radiation passes. The optical effects observed are often nontrivial in character and bear a profound physical meaning. Many phenomena observed by the naked eye occur in experiments on atmospheric laser sensing. For instance, in work [4] we describe the phenomenon of reflection of laser radiation ("green hotspots") from ice plates during wintertime atmospheric sensing (Fig. 1). The conditions of the experiments and the main technical characteristics of the lidar system used are presented in Tables 1 and 2.

From the analysis of lidar data we determined the characteristics of the layer of enhanced (specular) scattering. This layer was at an altitude of 160 m above the Earth's surface and had a thickness of 15 m. As can be seen from Fig. 2, the light traces reflected from ice crystals and intercepted by the Earth's surface differ in shape and intensity. After analysis of the images of traces, they can be divided into three types:

(1) a spot shaped as a circle 5—7 cm in diameter, uniformly illuminated throughout the surface (Fig. 2a);
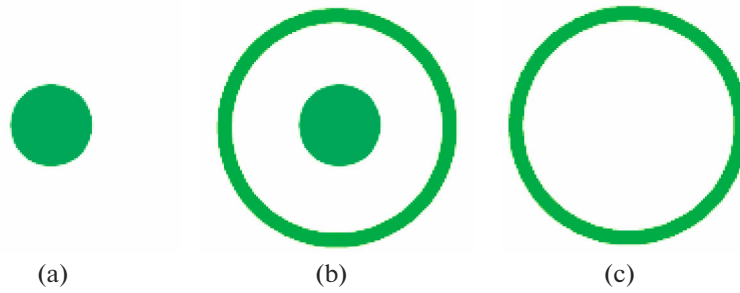
Fig. 2. Schematic image of the shapes of light spots on the Earth's surface.

(2) a similar spot (see point 1), but surrounded by a concentric ring 15−20 cm in diameter positioned symmetrically to the central spot (Fig. 2b);

(3) a similar spot (see point 2), but without central spot (Fig. 2c).

Before proceeding with the analysis of patterns of light spot formation, we will make a few comments.

(1) Effects will be considered exclusively within the wave theory of light.

(2) Effects observed in vitro (e.g., laboratory observations of Newton's rings in reflected light) can be translated into in situ conditions (i.e., into field conditions).

(3) All images of "light spots" on the Earth's surface were obtained near lidar under normal (or near-normal, with no more than 0.005-rad deviation from vertical) incidence of the light beam on the elements of reflecting layer; therefore, the path of beams in the reflecting layer is considered only for the case of normal light incidence on reflecting surfaces.

(4) Presumably, entities of all types are created by single regularly shaped scatterers (ice plates). In this case, we can consider dealing with point sources of radiation because reflecting elements have a characteristic transverse size of ∼0.1−0.5 mm, much smaller than the distance from reflecting layer to the Earth's surface (hundreds of meters).

Type 1 reflection. In this case, light traces appear as circularly shaped spots uniformly illuminated over the entire surface (Fig. 2a). This light trace is explained in Fig. 3.

We notice that $d \ll m$ in Fig. 3. It also should be kept in mind that d is on the order of the wavelength under real conditions. Assuming that $\Delta d = dn$, the condition of the maximal difference between the optical paths of beams *1* and *2* will be satisfied provided the equality

$$\Delta d_{\max} = 2k\frac{\lambda}{2}, \tag{1}$$

where $k = 1, 2, 3, \ldots$ is an integer positive number; λ is the wavelength of laser radiation, $\lambda = 0.53 \times 10^{-6}$ m is the laser radiation wavelength. In other words, an even number of half-waves of incident radiation should fit
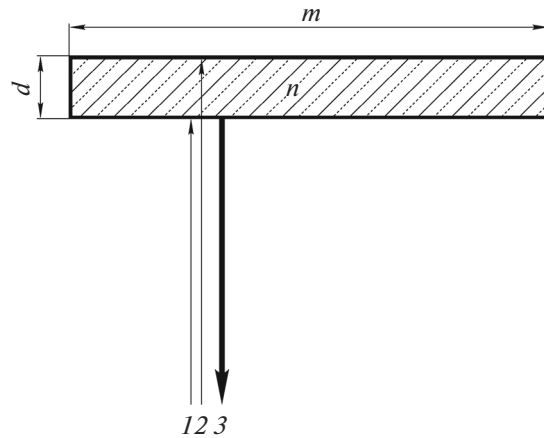

Fig. 3. Schematic illustration of flat ice plate: d is the thickness of plane-parallel ice plate; n is its refractive index; m is the transverse plate size; *1* and *2* are laser beams incident on the lower and upper facets, respectively; and *3* is the resulting reflected beam.

into the distance equaling the difference of the optical paths of beams *1* and *2*.

Another necessary condition for observing the interference pattern is the coherence of incident beams *1* and *2*. This condition is also satisfied because the thicknesses of reflecting ice plates are in the range $10^{-6}-10^{-5}$ m, which is obviously smaller than the spatiotemporal coherence even for a multimode laser.

Table 2. Technical characteristics of lidar system

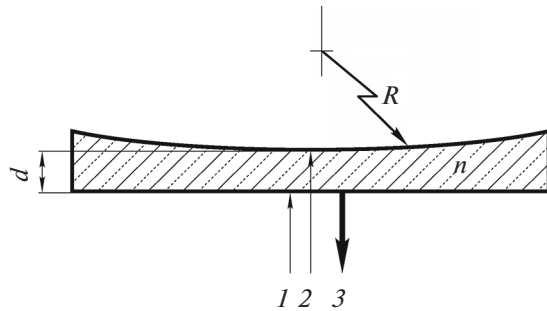| Characteristic	Value
Wavelength	0.53×10^{-6} m
Diameter of radiation source	0.1 m
Angular divergence of laser radiation	100 μrad
Laser pulse duration	10 ns
Photodetector type	FEU-84
Recording "green hotspots" on Earth's surface	Visual, or using photo camera

Fig. 4. Schematic illustration of reflection from lens-shaped ice plate. Notations are same as in Fig. 3; R is the radius of curvature of the upper plate surface.
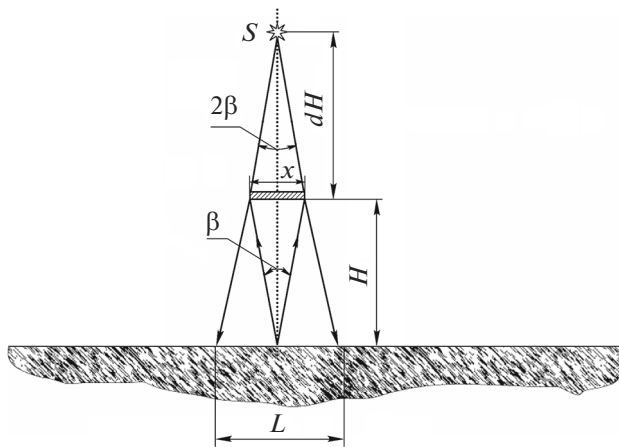

Fig. 5. Geometry of reflection from ice plate: β is the divergence of radiation source; S is a virtual image of the radiation source; H is the distance from the Earth's surface to the reflecting element; and dH is the distance from the reflecting layer to the virtual radiation source.

Another explanation for the occurrence of type 1 light trace can be because the upper ice facet is inclined relative to the lower one, so that beams *1* and *2* propagate along different optical paths without interfering with each other. In this case, the intensity of radiation reflected only from the lower facet and, hence, the brightness of light traces on the surface are much smaller because the intensity of the light wave is not amplified as a result of the summing of amplitudes.

Type 2 reflection. One of the hypotheses explaining the formation of light rings on the Earth's surface is based on the diffraction theory, i.e., the ring-shape structure is formed due to the Fraunhofer diffraction on the aperture of the source of radiation. At the same time, the diffraction angle [5]:

$$\varphi_d = 1.22 \frac{\lambda}{D}, \qquad (2)$$

where D is the aperture diameter of the laser transmitter. Obviously, $\varphi_d = 6.5 \times 10^{-6}$ rad since $D = 0.1$ m. For the

conditions of the experiment at an altitude of 320 m above the Earth's surface, taking into account the reflection effect, the radius of the first diffraction maximum is ~2.1×10^{-3} mm, which is inconsistent with the experimentally observed pattern where the ring diameters on the Earth's surface are 15–20 cm.

The hypothesis of the existence of ice plates with a lens-shaped structure can be invoked to explain the occurrence of type 2 light traces within the wave theory. This means that one (or both) ice plate facets is concave in shape (Fig. 4). The authors of work [6] consider in detail why ice plates with this geometry can occur. In this work, we also describe a possible way for ice plates to form with concave surfaces.

We will keep in mind that $d \sim \lambda$. In this case, for the optical difference Δd between paths, the condition of the maximum (of the light spot at the center) is given by formula (1); and the condition of minimum (the region between the central spot and the ring) is formulated as

$$\Delta d_{min} = (2k + 1)\frac{\lambda}{2}. \qquad (3)$$

Thus, the condition of the minimum is that an odd number of half-waves fits into the optical path difference between interfering beams.

A ring around the light spot occurs if the maximum condition holds but interference occurs between beams that are at a certain distance from the lens center. This distance is determined by the phase shift Δd for beams *1* and *2* as these beams move from the center to periphery until an even number of half-waves fits into Δd. As a result, a light ring is displayed (on the Earth's surface in our case).

It is important to note that the interference images thus observed are not localized in space (i.e., observed strictly at a certain point). The radius r_k of the ring on the Earth's surface can be calculated from the formula

$$r_k = G\left(\frac{(2\mu - 1)R\lambda}{2n}\right)^{1/2}, \qquad (4)$$

where G is the enlargement factor, which depends on the geometry of the experiment and is equal to the ratio of the size of annular structure observed on the Earth's surface to the size of the ring near the reflecting element; μ is the ring number; R is the radius of curvature of the reflecting element (ice crystal); and n is the refractive index of the reflecting element.

Summarizing, the light rings around the light spot at the center are the projections of interference pattern (Newton's rings) onto the Earth's surface enlarged due to finite divergence of laser radiation.

Based on Fig. 5, the G value can be calculated from the formula

$$\frac{H + dH}{dH} = \frac{L}{x} = G, \qquad (5)$$

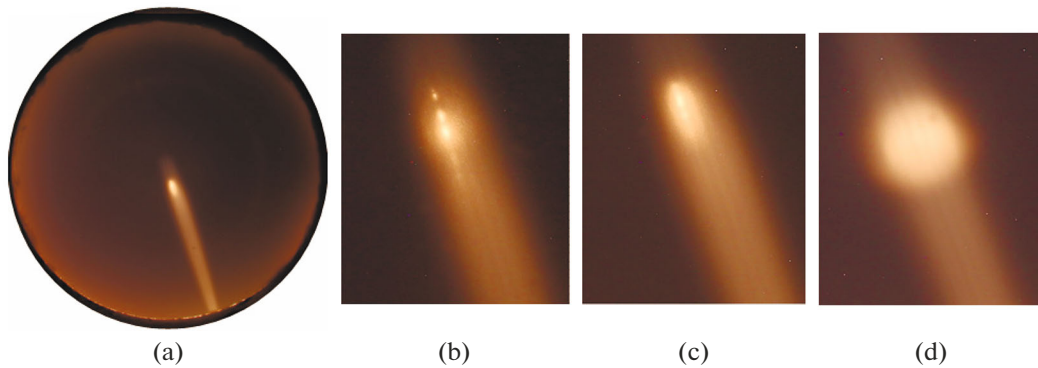|			
(a)	(b)	(c)	(d)

Fig. 6. Images of specular reflection in the case of searchlight sensing: (a) example of image recorded by AllSky system; (b–d) fragments of images with localized reflection of radiation from the specular layer.

where x is the size of the image of the ring near the reflecting plate; and L is the size of the image of the ring on the Earth's surface.

The absence of higher-order rings with $k > 1$ can be due to small sizes of reflecting ice plates. Indeed, the radius of the first ring at $R = 1$ m and $n = 1.31$ calculated from formula (4) without accounting for the enlargement factor is approximately 0.5 mm, which is close to the limiting size of ice plates residing in the atmosphere in a suspended state and floating in air. Larger particles are required for the occurrence of higher-order rings. However, it should be remembered that the particle mass is proportional to size cubed; therefore, larger plates rapidly sediment onto the Earth's surface thus contributing nothing to the light spot formation.

Type 3 reflection. A ring without a central spot is observed in this case. This type of reflection totally fits into type 2 reflection pattern; however, the condition of minimum (3) is satisfied for the central spot.

ALLSKY CAMERA OBSERVATIONS OF SPECULAR REFLECTION IN THE ATMOSPHERE

The presence of specular reflection is quite difficult to record during lidar sensing. In addition, it is almost impossible to estimate the extent of specular layers. Numerous remote sensing observations in many directions, i.e., in azimuths and elevation angles, are required to estimate the state of the atmosphere using lidar. The extensive specular layers can nevertheless be detected and localized. A high-resolution wide-angle system for observing the atmosphere-scattered optical radiation can be used for these purposes [7–9]. The IAO SB RAS staff had developed and successfully operated an automatic AllSky software-hardware system for monitoring the state of the atmosphere [10, 11]. This system enables round-the-clock observations and data processing for solving a number of tasks associated with monitoring of optical-physical state of the atmosphere.

Based on regular observations [12], layers with specular reflection can now be recorded with the system developed [13]. This phenomenon shows up most often over Tomsk in fall–winter, in a period of the most intense formation of temperature inversion layers, which presumably play a role of particle-retaining layers. Processing of images recorded and the relationship between the characteristic points on the terrain make it possible to estimate the altitude of specular cloud layer. Naturally, complex observations with lidar sensing systems are advisable for a more accurate determination of the specular layer altitude.

A powerful searchlight with low (~0.02 rad) beam divergence can be used together with simultaneous image recording by AllSky monitoring system to detect specular layers located at high (up to 1000 m) altitudes. After the searchlight radiation interacts with the aerosol particle layer, a diffuse glow of the searchlight-illuminated section of the aerosol layer occurs. A virtual image of the radiation source can be recorded when this layer possesses specular properties (Fig. 6).

It should be noted that the lidar sensing data confirmed the presence of the specular reflection layers observed in searchlight sensing and presented in Fig. 6. The lidar sensing showed that the specular reflection layers were in the altitude range from 98 to 365 m, which well correlates with searchlight sensing data.

CONCLUSIONS

Thus, based on our studies, we can draw the following conclusions.

(1) Spots of light reflected from the corresponding atmospheric layers can be observed on the Earth's surface near the radiation source, during laser sensing under certain conditions.

(2) The shapes and sizes of these spots make it possible to explain their occurrence by the interference theory.

(3) The wide-angle AllSky camera (IAO SB RAS) can be used to observe the occurrence in the atmosphere of specularly reflecting layers, which produce a number of nontrivial effects.

(4) Analysis of images obtained using searchlight and AllSky system allows estimating the altitude of a specular layer.

CONFLICT OF INTEREST

The authors declare that they have no conflicts of interest.

REFERENCES

1. *Thermodynamics of Atmospheres and Oceans,* Ed. by J.A. Curry and P.J. Webster (Academic Press, 1999). https://doi.org/10.1016/S0074-6142(99)80027-8

2. C. M. R. Platt, N. L. Abshire, and G. T. McNice, "Some microphysical properties of an ice cloud from lidar observation of horizontally oriented crystals," J. Appl. Meteorol. Climatol. **17** (8), 1220−1224 (1978).

3. O. A. Volkovitskii, L. N. Pavlova, and A. G. Petrushin, *Optical Properties of Ice-Crystal Clouds* (Gidrometeoizdat, Leningrad, 1984) [in Russian].

4. V. N. Marichev, V. P. Galileiskii, D. O. Kuz'menkov, and A. M. Morozov, "Experimental observation of the mirror reflection of laser radiation from oriented particles concentrated in the atmospheric layer," Atmos. Ocean. Opt. **23** (2), 128−131 (2009).

5. G. S. Lansberg. *Optics* (Nauka, Moscow, 1979) [in Russian].

6. K. G. Libbricht, "The physics of snow crystals," Rep. Prog. Phys. **68** (4), 855−895 (2005). https://doi.org/10.1088/0034-4885/68/4/R03

7. V. P. Galileiskii and A. M. Morozov, "All-sky photometric complex," Atmos. Ocean. Opt. **6** (9), 645−647 (1993).

8. O. S. Ugolnikov and I. A. Maslov, "Optical properties of the undisturbed mesosphere from wide-angle twilight sky polarimetry," Cosmic Res. **51** (4), 235−240 (2013).

9. E. Kassianov, C. N. Long, and J. Christy, "Cloud-base-height estimation from paired ground-based hemispherical observations," J. Appl. Meteorol. **44**, 1221−1233 (2005).

10. D. V. Kokarev, V. P. Galileiskii, A. I. Elizarov, and A. M. Morozov, RF Utility Patent No. 191 582 of Aug. 13, 2019.

11. V. P. Galileyskii, A. I. Elizarov, D. V. Kokarev, G. G. Matvienko, and A. M. Morozov, "Software and hardware system for monitoring and control of the optical-physical state of the atmosphere: Part 1: Panoramic optical station," Proc. SPIE—Int. Soc. Opt. Eng. **11916**, 119168K (2021). https://doi.org/10.1117/12.2603231

12. V. P. Galileyskii, A. I. Elizarov, D. V. Kokarev, G. G. Matvienko, and A. M. Morozov, "Software and hardware system for monitoring and control of the optical-physical state of the atmosphere: Part 2: Methods and algorithms for data processing," Proc. SPIE—Int. Soc. Opt. Eng. **11916**, 119168L (2021). https://doi.org/10.1117/12.2603233

13. A. M. Morozov, V. P. Galileiskii, A. I. Elizarov, and D. V. Kokarev, "Observation of the mirror reflection of lighted underlying surface by a cloudy layer of ice plates," Opt. Atmos. Okeana **30** (1), 88−92 (2017).

Translated by O. Bazhenov